Towards the Development of Photo-Reactive Ruthenium (II) Complexes Targeting Telomeric G- Quadruplex DNA

Justin Weynand, Aurélie Diman, Michaël Abraham, Lionel Marcélis, Hélène Jamet, Anabelle Decottignies, Jérôme Dejeu, Eric Defrancq, Benjamin Elias

Towards the Development of Photo-Reactive Ruthenium (II) Complexes Targeting Telomeric G-Quadruplex DNA

Justin Weynand,[a,b] Aurélie Diman,[c] Michaël Abraham,[a] Lionel Marcélis,[a] Hélène Jamet,[b] Anabelle Decottignies,[c] Jérôme Dejeu,[b] Eric Defrancq,*[,b] and Benjamin Elias*[,a]

[a] *Université catholique de Louvain (UCL), Institut de la Matière Condensée et des Nanosciences (IMCN), Molécules, Solides et Réactivité (MOST), Place Louis Pasteur 1, bte L4.01.02, B-1348 Louvain-la-Neuve, Belgium*

[b] *Université Grenoble-Alpes (UGA), Département de Chimie Moléculaire, UMR CNRS 5250, CS 40700, 38058 Grenoble, France*

[c] *Université catholique de Louvain (UCL), de Duve Institute, Avenue Hippocrate 75, 1200 Brussels, Belgium*

ABSTRACT

The design and characterization of new ruthenium(II) complexes aimed at targeting G-quadruplex DNA is herein reported. Importantly, they are based on oxidizing 1,4,5,8-tetraazaphenanthrene (TAP) ancillary ligands known to favour photo-induced electron transfer (PET) with DNA. Photochemistry of complexes **1-4** have been studied by classical methods and revealed the ability for two of them to photo-abstract an electron from guanine. From the studies of the interactions with DNA by using luminescence, circular dichroism, Bio Layer Interferometry and Surface Plasmon Resonance experiments, we demonstrated the selectivity of the complexes for telomeric G-quadruplex over duplex DNA. Preliminary biological studies of these complexes have been performed: two of them showed a remarkable photo-cytotoxicity towards telomerase negative U2OS osteosarcoma cells whereas very low mortality was observed in the dark, using the same photo-drug concentration.

Introduction

DNA is considered as an interesting target for developing novel classes of therapeutic agents. Until recently, the focus has been on double-stranded DNA structures (duplex DNA), in which two sequences of DNA are held together in an antiparallel double-helical architecture through canonical Watson-Crick A/T and G/C base pairing. Targeting duplex DNA has mainly been achieved by using intercalators (*i.e.*, small molecules that interact with DNA through intercalation between two adjacent base pairs) or groove binders (*i.e.*, small molecules that interact with DNA in the minor and/or major groove regions).[1] More recently, targeting alternative DNA architectures, in particular G-quadruplexes (G4s), has been increasingly pursued. G-quadruplexes DNA are secondary DNA structures found in guanine rich sequences. The basic unit is called G-quartet, which corresponds to the coplanar arrangement of four guanines held together by Hoogsteen hydrogen bonds and stabilized by physiologically abundant Na^+ or K^+ cations. G-quartets can stack to form G-quadruplexes DNA. G-quadruplexes can adopt a wide variety of topologies according to the number of strands involved in the structure, the strand direction, and variations in loop size and sequence.[2-4] Sequencing and bioinformatics analyses of the human genome indicate that it contains as much as 700,000 sequences of potential G-quadruplex structures (PQS). Interestingly, these putative G-quadruplex forming sequences are not distributed randomly in the genome. Indeed a statistically significant enrichment of PQS was found in several relevant domains of the human genome including the telomeric region and promoter regions of a number of genes such as the proto-oncogenes c-Myc, c-Kit, bcl-2, KRAS as well as in viruses.[5-6] Strong arguments have been recently provided that argue in favour of the formation of G-quadruplex DNA structures within cells by using G-quadruplex antibodies as well as binding-activated fluorescent G4-targeting ligands.[7-9] Several G4-binding regulatory proteins have been identified and G4 formation is now suspected to be involved in numerous pathogenic processes including degenerative disorders, oncogene regulation, and viral

infections. Altogether, these data are in agreement with a biologically relevant regulatory role for G-quadruplexes.

In this context, the biological functions of G4s are certainly the most documented for the telomeric region. Human telomeric DNA is made of a repeat of the sequence $^{5'}$TTAGGG$^{3'}$ and it is well admitted that telomeric DNA plays important roles in the development of cancer cells.[10-11] In healthy cells, the telomere shortens after each cell division and when a limit is reached (*i.e.,* Hayflick limit), the cell enters into senescence. Whereas in most cancer cells, the telomere length is maintained, leading to replicative immortality. Two different processes are involved in telomere maintenance: *(i)* the overexpression of the telomerase enzyme which adds copies of telomeric repeats at the chromosome ends,[12] and *(ii)* the homologous recombination-based mechanism, termed Alternative Lengthening of telomeres (ALT).[13-14] Telomerase overexpression is observed in almost 85% of cancer, whereas the ALT mechanism is active in 5-10% of the cases (in particular in osteosarcoma and glioblastoma).

Over the past decade, a number of small molecules (called G-quadruplex ligands), displaying varying degrees of affinity and more importantly selectivity (*i.e.* the ability to interact only with quadruplex DNA and not with duplex DNA), have been designed to target G-quadruplex DNA.[15-19] Most of these molecules have been built from an aromatic core, able to interact with G-quadruplex motifs through π-stacking, and decorated with substituents (often positively charged) that can interact with G-quadruplex grooves and/or loops for improving the affinity for G4s as well as the selectivity *versus* duplex DNA. G4 ligands approach is now considered to be a useful molecular tool to enhance and/or promote quadruplex-related biological effects in cells and shows high potential for future therapies.[20] To the best of our knowledge, very few studies have been devoted to the design of photo-reactive probes targeting G4s that could be interesting for phototherapy development. Freccero and Coll. have linked to the well-known naphthalene diimide (NDI) G4-ligand, a phenol moiety that produced phenoxyl radicals upon

irradiation.[21] They have showed the ability of such NDI-phenolate conjugate to kill MCF7 cancer cells after irradiation.

The design of new metal complexes targeting G-quadruplex DNA has gained an intense interest for their potential anticancer properties.[22-23] Indeed, some Pt(II),[24-28] Ni(II),[29-31] Ru(II)[32-34] or Ir(III)[35-37] showed good affinity and selectivity towards G4s. In comparison to organic compounds, metal complexes possess many advantages such as a net positive charge, tunable geometry and, more interestingly, some of them present interesting photochemical properties. In this context, polyazaaromatic ruthenium(II) complexes represent ideal candidates to target genetic material like G4s. Thanks to their optical properties including a large Stokes shift, good photo-stability, high quantum yield and long-lived luminescence, they have been developed to probe different DNA sequences,[38] such as mismatches,[39] abasic sites[40] or G4s.[32] More recently two ruthenium(II) complexes $[Ru(phen)_2(dph)]^{2+}$ and $[\{Ru(phen)_2\}_2(dph)]^{4+}$ based on dph ligand (dph = dipyrazino[2,3-a:2',3'-h]phenazine) have been reported to show a good selectivity towards G4s.[41] However, none of these reported compounds is able to photo-induce oxidative damages under light irradiation. Highly π-deficient ligands such as 1,4,5,8-tetrazaphenanthrene (TAP) are known to enhance the photo-oxidizing power of the resulting complexes.[42] Indeed, in the presence of DNA, a photo-induced electron transfer (PET) from a guanine (G) base towards the excited complex has been evidenced for ruthenium(II) complexes bearing at least two TAP ligands. This PET leads to dramatic consequences to the living cells: *(i)* the formation of adduct between the complex and the guanine or *(ii)* DNA photo-cleavage (type I photo-oxidation).[43-45] A photo-reaction process for bridging two guanine bases of a quadruplex oligonucleotide by the rigid dinuclear $[(TAP)_2Ru(tpac)Ru(TAP)_2]^{4+}$ complex has also been reported.[46]

In the present study, three new photo-oxidizing ruthenium(II) complexes (Scheme 1) that selectively target G-quadruplex DNA over duplex have been synthesized. They are based on the 2-(4-

chlorophenyl)-1H-imidazo[4,5-f][1,10]phenanthroline (CPIP) ligand, of which some ruthenium(II),[47] platinum(II)[48] or iridium(III)[36] complexes have been previously reported as selective DNA switch. However, none of them has the ability to induce a photo-electron transfer (PET) with guanine units. For this aim, the TAP moiety has been introduced in our ruthenium(II) complexes through different strategies (Scheme 1): *(i)* by incorporating two ancillary TAP ligands (complex **3**), *(ii)* by modifying the phenanthroline imidazole ligand with TAP (complex **2**), *(iii)* by combining both strategies (complex **4**). Complex **1** containing phen-based ligands was used as a reference. Steady-state luminescence, circular dichroism (CD), Bio Layer Interferometry (BLI) and Surface Plasmon Resonance (SPR) studies have been performed and demonstrated a good affinity for G-quadruplex DNA as well as selectivity *versus* duplex DNA. Preliminary biological studies of these complexes have been performed and revealed that two of them showed a remarkable photo-cytotoxicity towards U2OS osteosarcoma cells whereas very low mortality was observed in the dark, using the same photo-drug concentration.

Results and Discussion

Synthesis of complexes 1-4 (Scheme 1).

The planar ligand CPIP (X=CH) was synthesized by condensation of 4-chlorobenzaldehyde with 1,10-phenanthroline-5,6-dione in an ammonium media as previously reported in the literature.[36] The ligand CPITAP (X=N) was obtained according to a new protocol developed in our laboratory, using 4-chlorobenzaldehyde and 9,10-diamino-1,4,5,8-tetraazaphenanthrene. The reaction was carried out in a refluxing acetic acid/ethanol mixture, during 60 h. Purification by preparative SiO_2 chromatography afforded pure CPITAP ligand, which was characterized by ^{1}H, ^{13}C NMR spectroscopy and high-resolution mass spectrometry (HRMS) (see the Experimental Section and Figures S1, S2 and S11 in the Supporting Information). The corresponding Ru(II) complexes were synthesized by direct chelation of the N^N ligand onto a Ru(II) precursor bearing either 1,10-phenanthroline (phen, Y=CH) or 1,4,5,8-

tetraazaphenanthrene (TAP, Y=N) moieties (Scheme 1). The reactions were carried out in the dark and under argon to avoid photo dechelation and oxidation of the metal centre. Complexes **1-4** have been characterized by ^{1}H NMR spectroscopy and HRMS analyses (see the Experimental Section and Figures S3-10 and S12-15) as well as UV-vis, cyclic voltammetry (CV) and photochemical studies (*vide infra*).

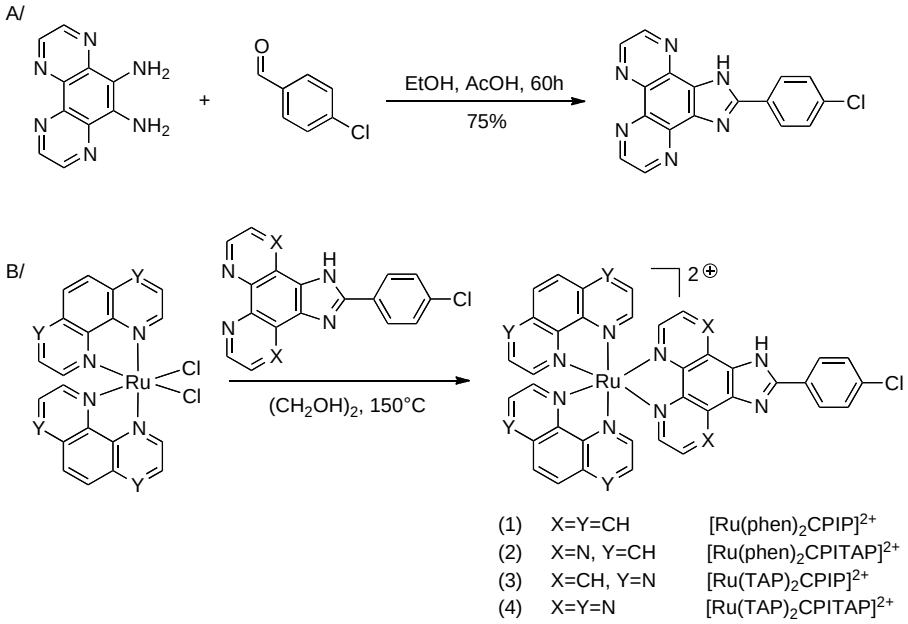

Scheme 1. *Synthesis of A/ CPITAP ligand and B/ Ru^{II} complexes **1-4**.*

Absorption and Luminescence Properties.

The absorption and luminescence data for complexes **1-4** are gathered in Table 1 and in Figures S16-19. For all complexes, the absorption bands in the UV regions were attributed to Ligand Centred (LC) transitions from comparison with literature data while the absorption maxima between 400 and 500 nm were ascribed to Metal to Ligand Charge Transfer (MLCT) transitions as previously shown for similar complexes.[49-50] Emission spectra were measured in acetonitrile and water, at room temperature and at 77 K in EtOH/MeOH mixture (4/1, v/v). Complexes **1-4** display a broad unstructured emission in organic solvent and water.

Table 1. Absorption and luminescence data for complexes **1**-**4**.

	λ_{Abs} (ε) [a]		λ_{Em} [b]		Φ_{Em} [c]		τ (ns) [d]	
Complex	CH_3CN	CH_3CN	H_2O	77K	CH_3CN	H_2O	CH_3CN	H_2O
1	460	597	603	570	0.009	0.069	115	572
	(1.61)				(0.058)	(0.14)	(380)	(1315)
2	488	671	704	612	0.011	0.0059	376	162
	(0.59)				(0.082)	(0.007)	(692)	(162)
3	471	623	641	598	0.037	0.017	686	629
	(1.11)				(0.138)	(0.011)	(1620)	(786)
4	451	586	600	565	0.01	0.0006	80	6
	(1.28)				(0.02)	(0.0005)	(78)	(6)

[a] λ in nm for the most bathochromic transition in MeCN (extinction coefficient, ε x 10^4 $M^{-1}cm^{-1}$). [b] λ in nm at RT in MeCN and H_2O and at 77K in EtOH/MeOH (4/1, v/v). [c] Quantum yield of emission measured by comparison with the reference $[Ru(bpy)_3]^{2+}$, under air and under argon (in brackets), excitation at 450 nm, errors are estimated to 10%.[51] [d] Luminescence lifetime (after irradiation at λ = 400 nm) measured under air and under argon (in brackets), errors are estimated to 5%.

The positive solvatochromism from acetonitrile to water and the hypsochromic shift of the emission band at 77K suggest a more polar excited state than that of the ground state, in agreement with the occurrence of a charge transfer (CT) upon irradiation, *i.e.* Metal to Ligand Charge Transfer (MLCT). The excited state energy decreases from **1** to **2**, in agreement with the stabilization of the LUMO localized on the imidazophenanthroline ligand, *i.e.* going from CPIP to the more electron-withdrawing CPITAP. A similar observation can be made for complexes **2** to **4**, for which the increased number of π-deficient ligands results in the stabilization of the metal-centred HOMO, leading to a more energetic transition. Comparison of luminescence lifetimes, under air and under argon allows us to conclude that all complexes are able to photosensitize oxygen, as previously reported in the literature for similar compounds.[52-53] It is also noted that luminescence quantum yield of complex **1** is lower in acetonitrile

than in water, consistent with data for $[Ru(phen)_3]^{2+}$ complex.[54] The relatively low luminescence of complex **2** to **4** in water is typical of TAP-based complexes and is generally attributed to increased non-radiative processes, likely due to interaction of the solvent with non-chelating nitrogen atoms (light switch effect). It should be also noted that complex **4** showed a very short excited state lifetime and a very low quantum yield of emission in water subsequently suggesting poor photo-induced damaging properties.

Electrochemical Study.

The oxidation and reduction potentials of complexes **1**-**4** were determined by cyclic voltammetry measurements in dry deoxygenated acetonitrile (Table 2 and Figures S20-23). Based on other similar Ru(II) complexes described in the literature, we can assume that complexes **1-4** display a one-electron oxidation wave. This corresponds to the oxidation of Ru(II) to Ru(III) as the anodic shift observed from **1** to **4** reflects the stabilization of the metal centred HOMO, due to the presence of highly π-deficient ligands (TAP) and consistent with the spectroscopic properties. For the reduction, each complex displayed several one-electron reduction waves, corresponding to the successive addition of electrons onto the ligands. The first reduction wave measured for **1** was attributed to the reduction of phen moieties of CPIP or ancillary ligands. As for complexes **2** to **4**, the first reduction wave, anodically shifted with respect to complex **1**, corresponds to the reduction of the TAP moiety of either CPITAP or ancillary ligand.

All these data suggest the following photo-physical scheme for this family of complexes: according to literature data and our results, we can safely conclude that the HOMO is metal centred and its relative energy depends on the respective ligands surrounding the metal. The more π-deficient ligands are chelated onto the metal centre, the less reducing the complex will be. As for the LUMO, it is centred on a ligand, confirming the MLCT nature of the excited state. From the cyclic voltammetry measurements

and the spectroscopic data, the oxidation and reduction potential of the excited state can be roughly estimated. Not surprisingly, complexes **3** and **4** display a strong photo-oxidizing power (+1.23 and +1.39 V *vs* Ag/AgCl, respectively). With these results in hands, we have tested whether a photo-induced electron transfer (PET) would occur in the presence of the most reducing building block of DNA G-quadruplex, *i.e.* a guanine residue (E_{ox}= +1.10V *vs* Ag/AgCl).[55]

Table 2. Electrochemical data of complexes **1-4.**

Complex	$E_{ox\ 1/2}$	$E^{*}_{ox}{}^{a}$	$E_{red\ 1/2}$	$E^{*}_{red}{}^{a}$
1	+ 1.37	-0.74	-1.30	+ 0.81
2	+ 1.63	-0.29	-0.77	+ 1.15
3	+ 1.83	-0.18	-0.78	+ 1.23
4	> 2	>-0.16	-0.77	+ 1.39

Data were measured at room temperature in MeCN with 0.1M Bu_4NClO_4 as the supporting electrolyte (V *vs* Ag/AgCl), complexes concentration = 0.8 mM, [a] Excited state potentials estimated from equations $E^{*}_{ox} = E_{½\ ox} - E_{0-0}$ and $E^{*}_{red} = E_{½\ red} + E_{0-0}$. The energy of the excited state, $E_{0\text{-}0}$, is estimated by Franck-Condon line-shape analysis of the emission spectrum at 298 K in CH_3CN (see SI, Table S1 and S2).

Luminescence Studies in the Presence of dGMP.

As mentioned in the introduction, G-quadruplex DNA is a guanine rich sequence present in the genome. Recently, we have reported on a new family of Ru complexes exhibiting a good affinity and selectivity towards G-quadruplex DNA.[41] However, these complexes are not sufficiently oxidizing in their excited state to trigger direct oxidative damages (type I photo-reactivity). Ruthenium(II) complexes bearing at least two TAP (=1,4,5,8-tetraazaphenanthrene) ligands are well known in the literature to photo-react with a guanine moiety upon irradiation. Therefore, the photo-reactivity of our complexes towards dGMP has been investigated by Stern-Volmer steady-state luminescence quenching experiments. As well established in the literature, the luminescence quenching of Ru(II)-TAP complex upon addition of dGMP is due to an electron transfer (ET) from dGMP to the complex at the excited state. According to

estimated E^{*}_{red} (Table **2**), complexes **1** and **2** should not be enough photo-oxidizing to undergo ET with dGMP (E_{ox}= +1.10V *vs* Ag/AgCl). As anticipated, no luminescence quenching was observed for those complexes in the presence of dGMP. In contrast, Stern-Volmer plot performed with complex **3** (Figure 1), showed a luminescence quenching in the presence of increasing dGMP concentration, with a high efficiency close to the diffusion limit (quenching rate constant = 2.63 $x10^{9}$ $M^{-1}.s^{-1}$). Based on thermodynamic data, this luminescence quenching can safely be ascribed to a PET from the guanine moiety to the excited state of complex **3** (eq **1**).

$[Ru]^{2+}* + G \rightarrow [Ru]^{1+} + G^{\bullet+}$ (1)

Considering the oxidation power of the excited state of **3** and using the empirical Rehm-Weller equation, it is expected that process (1) will be exergonic by about -0.13 eV. In the case of **4**, PET should also be favoured by about -0.29 eV, but the poor luminescence properties of this complex did not allow any luminescence quenching experiments.

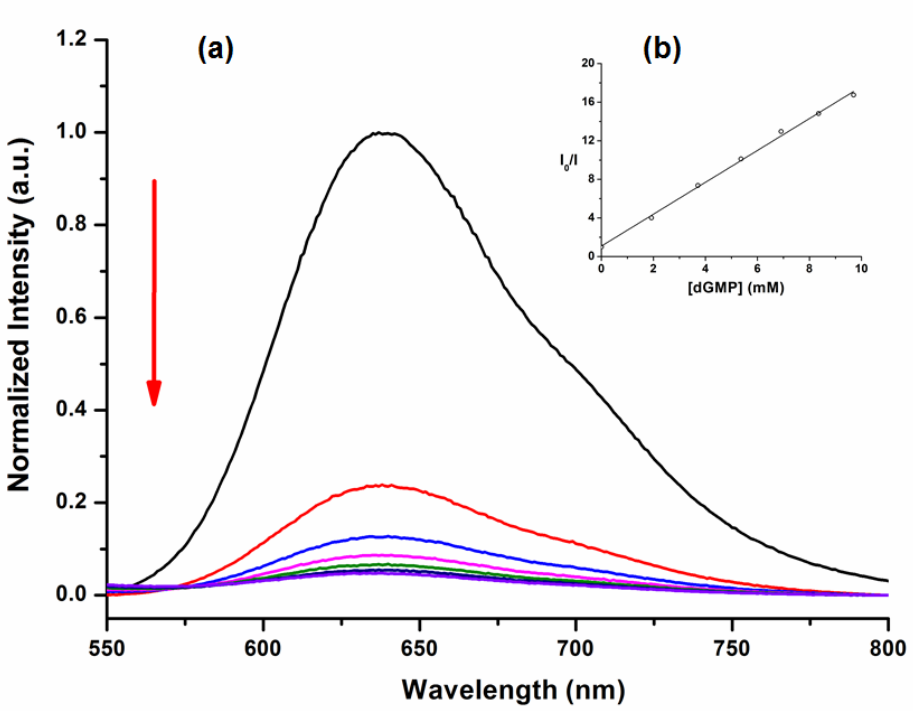

Figure 1. Luminescence quenching of complex **3** in the presence of dGMP (a) Emission spectra of complex **3**

upon increased concentration of dGMP. (b) Stern-Volmer plot. Complex concentration: 50 μM in Tris-HCl buffer (50 mM at pH = 7.4). Addition of dGMP from 0 mM to 10 mM. Excitation was performed at λ = 430 nm.

Luminescence Studies in the Presence of ODNs.

Due to the ability of complexes **1-3** to emit light in aqueous solvent, monitoring the luminescence upon addition of increased concentrations of oligonucleotides (ODNs) can be achieved. Experiments were performed with human telomeric wtTel23 ($^{3'}$TT(GGGATT)$_3$GGG$^{5'}$) and a GC rich hairpin sequence ($^{3'}$(GC)$_4$TTTT(GC)$_4^{5'}$). The experiments were carried out in 10 mM HEPES (pH 7.4), 35 mM NaCl, 50 mM KCl buffer in which the desired DNA structures (*i.e.* duplex or G-quadruplex) were formed (Figure S32). According to the redox properties of the complex, two behaviours can be observed upon addition of ODN: *(i)* an increase of the luminescence due to protection of the ruthenium(II) probe from the solvent in the hydrophobic environment of ODN or *(ii)* a decrease of luminescence resulting from a PET with a neighbouring guanine. Figures 2a,b show the enhancement of the luminescence through the addition of increasing amounts of wtTel23 or hairpin ODN for complexes **1** and **2**. This behaviour is consistent with (*i*) the protection of the complex by the ODN that decreases the rate of non-radiative processes, (*ii*) the fact that no luminescence quenching has been monitored in the presence of guanine moieties (*vide supra*). In contrast, the luminescence of complex **3** was quenched through the addition of increasing amounts of DNA (Figure 2c), attributed to a PET in agreement with the Stern-Volmer plots.

The above results from steady-state luminescence studies with complexes **1**-**3** suggested that a strong interaction between DNA and the complexes occurred. We thus decided to further investigate the interactions of the complexes with DNA in order to evaluate whether they display a specific affinity towards G-quadruplex structures over double-stranded DNA.

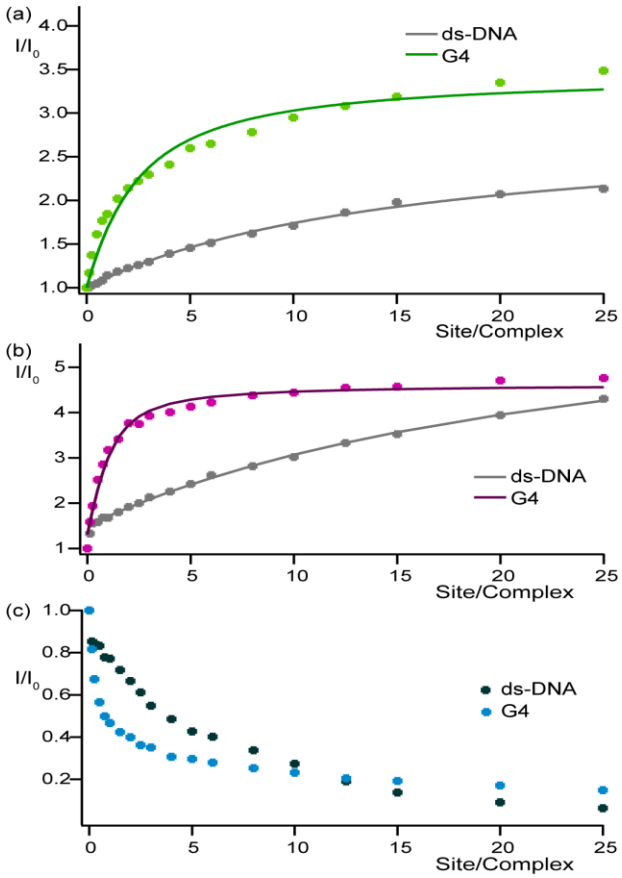

Figure 2. *Luminescence titration of complexes **1-3** by DNA.* Luminescence titrations of complexes **1, 2** and **3** (figures (a), (b) and (c), respectively) were carried out in 10 mM HEPES (pH 7.4), 35 mM NaCl, 50 mM KCl buffer by increasing proportions of ds-DNA (GC rich hairpin duplex $^{3'}(GC)_4TTTT(GC)_4^{5'}$, base pairs equivalents per Ru complex) or G-quadruplex DNA (wtTel23, $^{3'}TT(GGGATT)_3GGG^{5'}$, G-quartet equivalents per Ru complex). Solid lines obtained by a modified McGhee–von Hippel fitting process (see the SI) to evaluate the binding affinities. Excitation was performed at λ = 450 nm.

DNA Binding Analysis.

Different biophysical techniques including FRET-melting, UV-visible spectrophotometry, circular dichroism (CD), NMR and SPR have been developed for studying G-quadruplex DNA/ligand interactions.[17] In our case, the use of UV-visible absorbance was found unsuitable to study the binding affinity. Modifications of the absorption spectra of complexes were indeed detected upon addition of increasing concentrations of G-quadruplex DNA (Figure S24-31) but they were relatively moderate and

thus it was tedious to measure a binding affinity. Binding affinities of complexes **1**-**2** for G-quadruplex and duplex DNA can be also estimated by fitting the variation of luminescence intensity *versus* the ratio of binding site per complex (Figure 2). Complex **1** showed an apparent dissociation constant (K_D) of 77 µM for duplex DNA and 6.5 µM for G-quadruplex. The difference of binding affinities for duplex and G-quadruplex DNA is more drastic for complex **2** with K_D values of 123 µM and 2 µM, respectively. Only qualitative conclusions can be made about the affinity of complex **3** for wtTel23 G-quadruplex *versus* GC rich hairpin DNA, since a dynamic quenching process is also taking place, which should alter the luminescence intensity. However, it can be observed that the slope of the curve is steeper with G-quadruplex structure than with duplex DNA, indicating that the binding affinity is certainly stronger for the former one. We thus evaluated the affinities of these complexes towards DNA by means of CD melting assays, Bio Layer Interferometry (BLI) and Surface Plasmon Resonance (SPR).

CD melting assays

The ability of complexes **1**-**4** to interact with G-quadruplex DNA was first investigated by CD experiments. CD analyses were carried out in 10 mM Tris-HCl, 100 mM NaCl buffer or 100 mM KCl. As anticipated in 100 mM NaCl containing buffer conditions, wtTel23 folded into an antiparallel topology characterized by two positive peaks at 242 nm and 294 nm, respectively and a negative peak at 262 nm (Figure S33). Upon addition of complexes **2**-**4**, minor change in the ellipticity of wtTel23 was observed suggesting that these complexes do not induce major structural changes of the antiparallel conformation of G-quadruplex (Figure S33). For complex **1,** we also observed the appearance of a shoulder at 270 nm that could be explained by a slight modification of the topology induced by this complex (presence of hybrid II-type G4 folding). In 100 mM KCl containing buffer conditions, wtTel23 folded into a hybrid II-type G4 featured by a maximum at 290 nm and a shoulder at 270 nm (Figure S34). Again, minor change in the ellipticity of wtTel23 was observed thus revealing no major structural

changes upon binding. In the same way, the duplex structure ($^{5'}CGT_3CGT_5ACGA_3CG^{3'}$ hairpin) was not affected as no change in the CD spectra was observed upon addition of complexes **1-4** (Figure S35).

Table 3. Melting temperatures (T_m) of wtTel23 and duplex hairpin in the absence or presence of ligands (5 equiv).

	T_m (°C) (±1)	
Complex	wtTel23	hairpin
No ligand	52.9 (61.9)	68.7
1	58.5 (76.0)	58.0
2	58.0 (64.0)	67.6
3	57.3 (67.0)	68.1
4	52.9 (61.9)	67.2

WtTel23 sequence $^{3'}TT(GGGATT)_3GGG^{5'}$ was first annealed by heating at 95°C for 5 min in Tris-HCl buffer (10 mM, pH 7.04) with 100 mM NaCl or 100 mM KCl (in brackets) and cooled down overnight to room temperature. Oligonucleotides concentration = 2.5 μM. Hairpin sequence $^{5'}CGT_3CGT_5ACGA_3CG^{3'}$ was first annealed by heating at 95°C for 5 min in Tris-HCl buffer (10 mM, pH 7.04) with 100 mM NaCl and cooled down overnight to room temperature. The ellipticity was recorded at 290 and 252 nm for wtTel23 and duplex hairpin, respectively.

We then performed CD melting assays to evaluate whether complexes **1-4** induced stabilizing or destabilizing effects on the G-quadruplex and hairpin duplex DNA structures. CD melting curves were recorded in the absence or the presence of each complex (at 5:1 complex/DNA ratio) in 100 mM NaCl or 100 mM KCl containing buffers (Table 3 and Figures S36 and S37) in case of wtTel23 and in 100 mM NaCl containing buffer for hairpin duplex (Table 3 and Figure S38). CD melting experiments results clearly showed that complexes **1-3** induced a slight stabilization of wtTel23 whereas all the complexes do not significantly affect the stability of duplex DNA structures. Melting temperature assays thus confirmed the ability of most of the investigated complexes to selectively interact with G-quadruplex DNA *versus* duplex DNA. It should be mentioned that each complex is a racemic mixture of two enantiomers and that a preferential binding or a different binding mode of each enantiomer could exist. However the separation of both enantiomers represents a new and challenging task. Thus, we are

presently unable to comment on whether the changes observed by CD are due to different binding mode of each enantiomer. Because this technique is not the most appropriate for direct measurements of affinity constants, we next performed BLI analysis, which allowed us to determine the thermodynamic parameters for the interaction.

Bio Layer Interferometry studies

BLI is a label-free method for measurements of affinity constants, which allows the determination of the kinetics parameters of the interaction (such as SPR) and has been used to study biomolecular interactions between large biomolecules like protein-membrane interactions.[56] Until recently, we employed SPR analysis method based on the use of a Template Assembled Synthetic G-Quadruplex (TASQ) that allows precise control of G-quadruplex topology through assembly of constrained structures on a template.[57-61] We have adapted this SPR method for BLI. Different G-quadruplex features were used: intermolecular-like G-quadruplex motif **A** constrained in a parallel G-quadruplex topology, intramolecular G-quadruplex **B** (HTelo sequence in an equilibrium between the different topologies), human telomeric sequence (HTelo) **C** constrained in antiparallel topology, and hairpin DNA **D** (Figure 3). All the systems **A-C** formed the desired G-quadruplex structure in the conditions used for BLI analysis (10 mM HEPES pH 7.4, 35 mM NaCl, 50 mM KCl).[57-58]

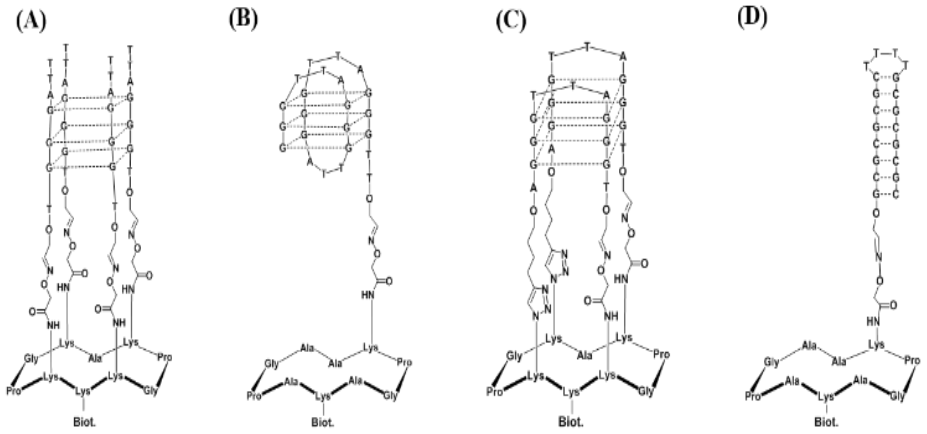

Figure 3. *G-quadruplex systems **A**-**C** and duplex control **D** used for Bio Layer Interferometry studies.* (**A**) parallel-stranded quadruplex (intermolecular like G-quadruplex); (**B**) intra quadruplex (intramolecular like G-quadruplex); (**C**) antiparallel human telomeric sequence and (**D**) duplex (hairpin).

Each evaluated complex showed K_D values in the micromolar range for G-quadruplex topologies **A**, **B** and **C** (Table 4 and Figures S39-42). These values fall within the range of those reported for related ruthenium(II) complexes interacting with G-quadruplexes. It is noticed that the substitution of carbon atoms by nitrogen atoms on the ligand (*i.e.* two Phen ligands in **1** replaced by two TAP ligands in **3** or CPIP ligand in **1** replaced by CPITAP ligand in **2**) only weakly affects the interaction with G-quadruplex. More interestingly, each ruthenium(II) complex showed a higher affinity for G-quadruplex structures than for duplex DNA. Indeed it was impossible to measure a K_D for interaction with duplex system **D** within the concentration range used in this study (*i.e.* from 5 to 40 µM) that suggests K_D values higher than 1 mM for duplex DNA **D** bound to each complex. The good selectivity was further confirmed by SPR analysis by using systems **B** and **D**. We obtained K_D values for the G-quadruplex system **B** of the same order of magnitude as for BLI analysis whereas none of the complex showed an affinity with duplex DNA **D** within the used concentration range (Figure S43 and Table S3).

Table 4. Data for the interaction of complexes **1-4** with DNA structures **A-D** from BLI analyses.

		Complex			
DNA structure	Constants	**1**	**2**	**3**	**4**
A	k_{on} (10^3 $M^{-1}s^{-1}$)	2.2 ± 1.3	9.4 ± 1.4	27 ± 1.2	8.0 ± 2.1
	k_{off} (10^{-1} s^{-1})	1.8 ± 0.5	2.9 ± 0.3	3.7 ± 0.6	13 ± 0.2
	K_D (µM) [a]	80 ± 20	31 ± 8	20 ± 11	182 ± 74
B	k_{on} (10^3 $M^{-1}s^{-1}$)	5.9 ± 1.6	130 ± 0.1	100 ± 1.0	27 ± 1.3
	k_{off} (10^{-1} s^{-1})	0.37 ± 0.8	1.5 ± 0.1	1.5 ± 1.4	4.6 ± 3.0
	K_D (µM) [a]	6.0 ± 4.0	1.0 ± 0.5	2.0 ± 0.5	22 ± 10
C	k_{on} (10^3 $M^{-1}s^{-1}$)	22 ± 1.0	62 ± 1.2	280 ± 1.6	61 ± 1.7
	k_{off} (10^{-1} s^{-1})	1.6 ± 0.4	1.8 ± 0.1	2.4 ± 0.8	9.4 ± 1.6
	K_D (µM) [a]	8.0 ± 2.0	3.0 ± 0.5	1.0 ± 1	10 ± 8
D	k_{on} (10^3 $M^{-1}s^{-1}$)	*nd* [b]	*nd* [b]	*nd* [b]	*nd* [b]
	k_{off} (10^{-1} s^{-1})	*nd* [b]	*nd* [b]	*nd* [b]	*nd* [b]
	K_D (µM) [a]	*nd* [b]	*nd* [b]	*nd* [b]	*nd* [b]

[a] Equilibrium dissociation constants deduced from the kinetic rate constants. [b] Due to very low binding of the different complexes with hairpin DNA the kinetic of the interactions could not be determined (*nd*) in the studied range of concentrations. This has been confirmed by SPR analysis (Figure S43). Running buffer: 10 mM HEPES pH 7.4, 35 mM NaCl, 50 mM KCl.

It was also noticed that the affinity of complexes **1-4** is higher for G-quadruplex structures **B** and **C**, which contain TTA loops in contrast with parallel-stranded quadruplex **A**. This is in agreement with interactions of the complexes with G-quadruplexes through mixed π-stacking over the guanine tetrad and further interactions with loops and grooves (see modelling part). To obtain further information of the affinity of complexes **1-4** for G-quadruplex, the association (k_{on}) and dissociation (k_{off}) constants of the interaction were determined (Table 4) and again revealed the relatively low influence of the replacement of carbon by nitrogen atoms in complexes **1-4**. Indeed for a given G-quadruplex structure, k_{on} and k_{off} differ only slightly.

For the most biologically relevant G-quadruplex structure **C**, k_{on} and k_{off} values were also compared with those of well-known compounds that interact with G-quadruplex (*i.e.* pyridostatine PDS, Phen-DC3, BRACO-19, MMQ1 and TMPyP4).[61]

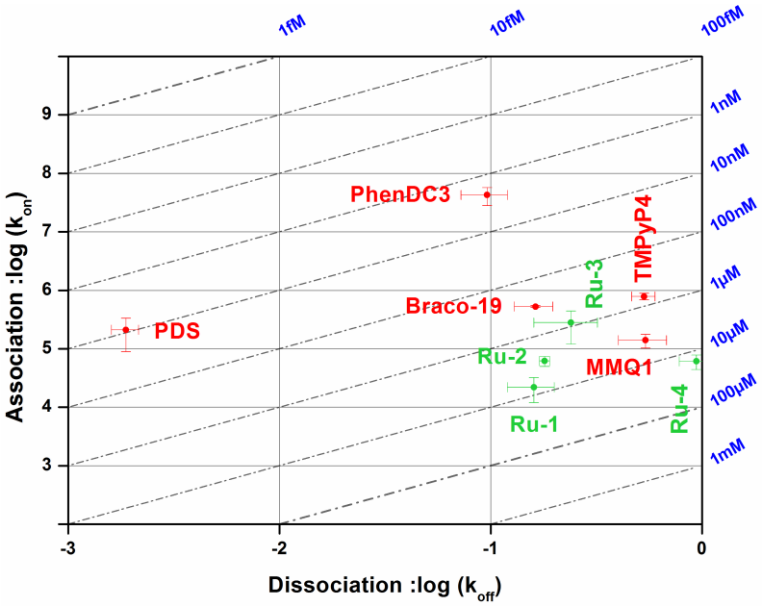

Figure 4. *Isoaffinity plot and kinetic characterization for G-quadruplex structure **C***. For $PhenDC_3$, BRACO-19, MMQ_1 and $TMPyP_4$ (in red) the analyses were performed by SPR;[61] for ruthenium(II) complexes (in green) from BLI analysis. K_D (parallel diagonal lines), k_{on} (association kinetic constant, y axis), k_{off} (dissociation kinetic constant, x axis).

As illustrated in Figure 4, complexes **1**-**4** display association and dissociation rates that are similar to those of BRACO, MMQ1 and TMPyP4. In particular the fact that our complexes showed similar affinity than BRACO-19, which has demonstrated anticancer activity through the stabilization of G-quadruplex at the telomere,[62] prompted us to study their photo-toxicity.

Molecular Modelling.

To obtain further insights into the interactions with G-quadruplex DNA, molecular docking calculations were carried out. The most interesting complex **3** (due to its photophysical properties) was docked to the human telomeric DNA structure (PDB entry 1KF1, wtTel23 in parallel conformation). From analysis of

the best-ranked docked positions, two binding modes were obtained (Figure 5). The first one consisted in a π-stacked positioning of **3** over the guanine tetrad while the second one showed an insertion of the complex into the TTA loop of G-quadruplex *via* the CPIP ligand. The initial calculations have been performed with the Δ-isomer of complex **3** to afford the two best-ranked positions in Figure 5. However, similar docked positions have been obtained with the other Λ enantiomer (see Figure S44 in the supporting information).

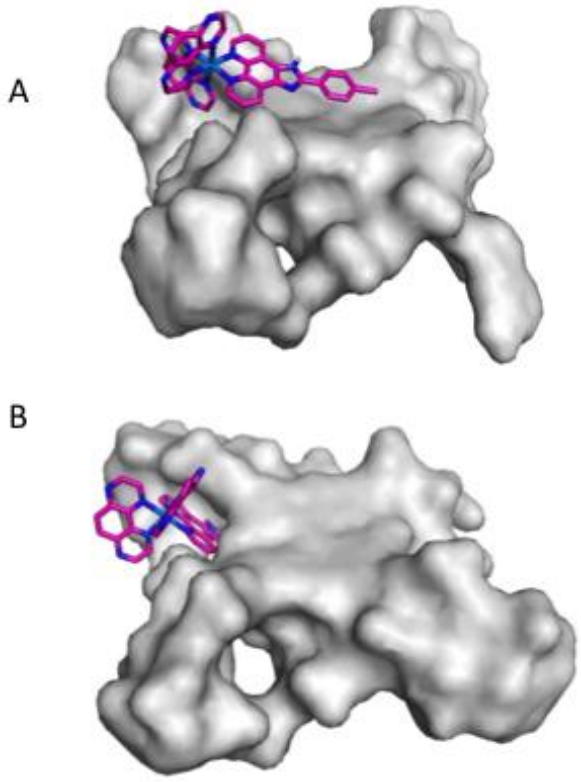

Figure 5. *Molecular modelling for the interactions of complex **3** (Δ-isomer) with G-quadruplex DNA.* Docking calculations for interaction of complex **3** with G-quadruplex human telomeric DNA structure (PDB entry 1KF1). (**A**) in π-stacked positioning over the guanine tetrad, (**B**) interaction with TTA loop.

Molecular mechanics dynamic simulations were then carried out in order to assess the stability of those two docking positions. For both of them, the complexes remained tightly bound in their relative positions (either in interaction with the TTA loop, or π-stacked) for up to 20 ns, thus emphasizing on the

strong affinity displayed by **3** towards G-quadruplex DNA. These results are consistent with BLI experiments. Indeed, the affinity of complex **3** with structure **A** (*i.e.* without loop) is lower than with both structures with loop (K_D of 20 µM for **A** while K_D is around 2 µM for **B** and **C**) that confirms the importance of the second docked position (*i.e.* loop interactions).

Cell Penetration.

Thanks to the ability of complex **1** to emit light in aqueous solvent, this one was studied by confocal microscopy to investigate the penetration into U2OS osteosarcoma cells.[63] Incubation was carried out during 24 h at 20 µM. As shown in Figure 6, complex **1** showed an efficient penetration in the cell, including the nucleus.

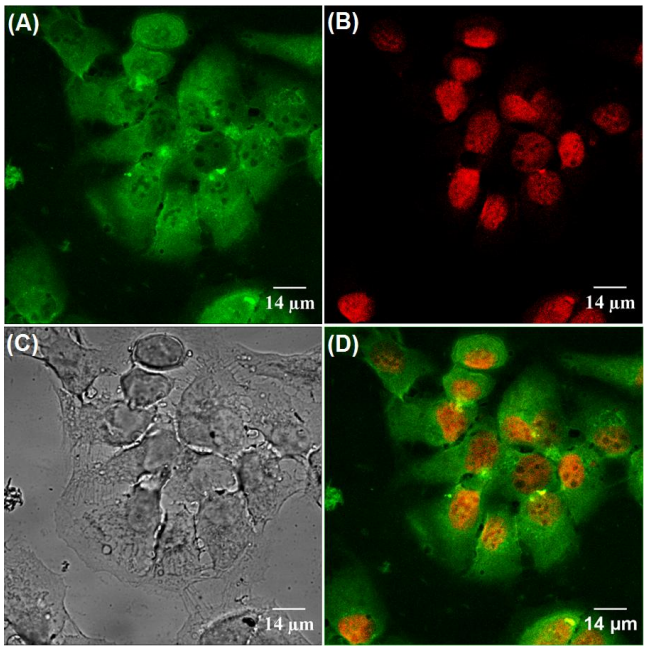

Figure 6. *Cell penetration study.* Fluorescence microscopy images of U2OS cells after incubation with 20 µM of complex **1** for 24 h, DMEM buffer. (**A**) Ru(II) complex in green (**B**) the nucleus in red, stained by Draq5 (**C**) Bright-field and (**D**) merged image. Scale 14 µm.

Photo-Cytotoxicity.

Preliminary photo-cytotoxicity studies were performed with complexes **1-4** on U2OS osteosarcoma cells. Figure 7 depicts the percentage of metabolically active cells after incubation of the cells with 10

µM of complexes **1-4** for 24 h and subsequent irradiation for 30 minutes (orange bars). Non-irradiated controls were also performed (blue bars). Interestingly, non-irradiated cells displayed very low rates of mortality whereas irradiation of the cells was associated with a dramatic decrease in survival. Indeed, 100% of mortality was obtained at 10 µM for complexes **1** and **3**, while complex **2** was slightly less efficient with 70% of mortality. As anticipated, complex **4** showed a very weak photo-toxicity in comparison with non-irradiated control cells. The strong photo-toxicity of complex **3** was confirmed by microscopic observations of the cells revealed by the tetrazolium salt-based metabolic assay that showed massive cells death upon irradiation (dead cells are clearly recognized by the change in shape, see Figure S45).

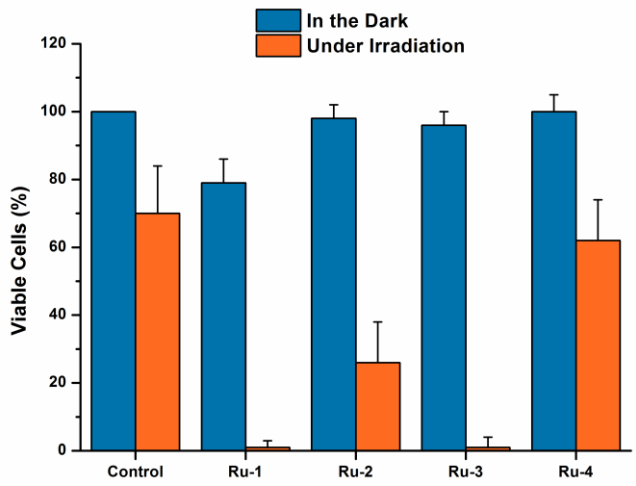

Figure 7. *Cell viability studies.* Percentage of viable U2OS cells after incubation with complexes **1-4** for 24 h in the dark followed by 30 min of irradiation (orange bar chart) or not (blue bar chart). The tetrazolium salt-based WST-1 assay was performed 24 h after irradiation. Values were normalized to untreated and non-irradiated U2OS cells. Error bars indicate SD.

A possible explanation of the photo-toxicity of **1-3** is that the internalized ruthenium complexes should photo-react with the biological material through type I photo-reaction (*i.e.* photo-electron transfer) or type II photo-reaction (singlet oxygen photosensitization), both mechanisms of photoreaction being

likely to induce DNA damages, ultimately leading to cell death. Contrariwise, the low photo-cytotoxicity of **4** more likely originates from its short excited-state lifetime, resulting in a poor photo-damaging ability.

Conclusion

A series of new ruthenium(II) complexes have been designed to target and photo-react with G-quadruplex DNA through the incorporation of CPIP ligand (or similar). As anticipated, the photophysical properties of the complexes are consistent with MLCT transitions and a metal centred HOMO. Consequently, these complexes are able to react with DNA through type II photoreaction (*i.e.* formation of singlet oxygen) or through photo-induced charged transfer (PET). All four designed complexes **1-4** displayed a good affinity for G-quadruplex DNA and selectivity *versus* duplex DNA. Docking based studies and molecular dynamic simulations revealed that this affinity is due to a π-π stacking above the tetrad and an interaction with the TTA loop.

Strikingly both complexes **1** and **3** were associated with dramatic photo-cytotoxic effect as 100% of mortality was obtained upon irradiation of U2OS osteosarcoma cells whereas very low mortality was observed in the dark, using the same drug concentration. These studies will be completed in the future to know whether this photo-cytotoxic effect is mainly due to a type II photoreaction (i.e. singlet oxygen photosensitization) or type I photoreaction (i.e. photo-induced charged transfer (PIET). Further experiments are currently performed to investigate whether telomeric DNA damages are induced into cells by complexes **1** and **3**. Interestingly, this photo-cytotoxicity should not involve the inhibition of telomerase activity through the stabilization of G-quadruplex as U2OS osteosarcoma cells do not express the telomerase enzyme. To the best of our knowledge, this would be the first example of high photo-cytotoxicity based on the use of metal complexes targeting telomeric DNA, through a mechanism, which does not involve the inhibition of telomerase. Therefore the photo-cytotoxicity of

these two complexes will be also evaluated towards either telomerase-expressing cancer cells or normal non-immortalized cells.

Experimental Section

Material and methods.

$[Ru(phen)_2Cl_2]$,[64] $[Ru(TAP)_2Cl_2]$,[42] 1,10-phenanthroline-5,6-dione,[65] 9,10-diamino-1,4,5,8-tetraazaphenanthrene[66] and 2-(4-chlorophenyl)-1H-imidazo[4,5-f][1,10]phenanthroline(CPIP)[48] were synthesized according to previously described literature protocols. The oligonucleotides wtTel23 ($^{3'}TT(GGGATT)_3GGG^{5'}$), GC rich hairpin duplex ($^{3'}(GC)_4TTTT(GC)_4{}^{5'}$) and hairpin duplex sequence $^{5'}CGT_3CGT_5ACGA_3CG^{3'}$ were prepared by standard automated solid phase oligonucleotide synthesis on a 3400 DNA synthesizer. After purification by RP-HPLC, they were thoroughly desalted by size exclusion chromatography (SEC). All solvents and reagents for the synthesis were of reagent grade and were used without any further purification. All solvents for the spectroscopic and electrochemical measurements were of spectroscopic grade. Water was purified with a Millipore Milli-Q system. ^1H and ^{13}C NMR experiments were performed in $CDCl_3$ or CD_3CN on a Bruker AC-300 Avance II (300 MHz) or on a Bruker AM-500 (500 MHz) at 20°C. The chemical shifts (given in ppm) are measured *vs* the residual peak of the solvent as the internal standard. High-resolution mass spectrometry (HRMS) spectra were recorded on a Q-Extractive orbitrap from ThermoFisher using reserpine as internal standard. Samples were ionized by electrospray ionization (ESI; capillary temperature = 320°C, vaporizer temperature = 320°C, sheath gas flow rate = 5 mL/min).

Synthesis.

2-(4-chlorophenyl)-1H-imidazo[4,5-f]pyrazino[2,3-h]quinoxaline **(CPITAP).** A solution of 9,10-diamino-1,4,5,8-tetraazaphenanthrene (53 mg, 0.250 mmol), 2-(4-chlorophenyl)-1H-imidazo[4,5-

f][1,10] phenanthroline (35 mg, 0.250 mmol) and EtOH (2.5 mL) were heated at reflux for 24h. Then acid acetic (3 mL) was added and the mixture was heated at 110°C for 60h. After cooling, acid acetic was evaporated under vacuum. The crude dark green solid was then purified over preparative SiO_2 chromatography ($CHCl_3$/EtOH 99/1) to afford pure CPITAP ligand as a yellow powder (62 mg, 75%). ^{1}H-NMR (300 MHz, $CDCl_3$): δ (ppm) 9.13 (d, 2H, J=1.8 Hz), 9.06 (d, 2H, J=2.0 Hz), 8.24 (d, 2H, J=8.6 Hz), 7.52 (d, 2H, J=8.6 Hz). ^{13}C-NMR (75 MHz, $CDCl_3$): δ (ppm) 151.71, 151.70, 145.73, 145.72, 143.79, 139.52, 137.6, 129.63, 129.62, 128.13. HR-MS Calcd for $C_{17}H_{10}N_6Cl$: 333.06500 Da, found 333.06489 Da.

$[Ru(phen)_2CPIP].2PF_6$ **1.** $[Ru(phen)_2Cl_2]$ (20 mg, 0.037 mmol) and CPIP (15 mg, 0.045 mmol) were dissolved in ethylene glycol (3 mL) and heated at 120°C for 20h in the dark and under argon. After cooling and addition of aqueous solution of NH_4PF_6, a solid was formed. The latter was washed 3 times with water, EtOH and Et_2O to afford the final pure product as an orange powder (36 mg, 90%). ^{1}H-NMR (500 MHz, CD_3CN): δ (ppm) 9.05 (d, 1H, J = 8.2 Hz), 8.89 (d, 1H, J = 8.4 Hz), 8.59 (dd, 4H, J = 8.3 Hz, J = 1.2 Hz), 8.28 (d, 2H, J = 8.7 Hz), 8.25 (s, 4H), 8.07 (dd, 2H, J = 10.5 Hz, J = 4.8 Hz), 8.01 (d, 2H, J = 5.4 Hz), 7.96 (d, 2H, J = 5.2 Hz), 7.67-7.59 (m, 8H). HR-MS Calcd for $C_{43}H_{27}N_8ClF_6PRu$ (**1** - $1PF_6$): 931.07595 Da, found 931.07688 Da.

$[Ru(phen)_2CPITAP].2PF_6$ **2.** $[Ru(phen)_2Cl_2]$ (20 mg, 0.037 mmol) and CPITAP (15 mg, 0.044 mmol) were dissolved in ethylene glycol (3 mL) and heated at 120°C for 20h in the dark and under argon. After cooling and addition of aqueous solution of NH_4PF_6, a solid was formed. The latter was washed 3 times with water, EtOH and Et_2O to afford the crude product. Purification over preparative SiO_2 chromatography ($CH_3CN/H_2O/NH_4Cl_{(sat)}$ 4/4/1, v/v/v) gave the final product as a red powder (18 mg, 64%). ^{1}H NMR (500 MHz, CD_3CN): δ (ppm) 8.86 (d, 2H, J = 2.9 Hz), 8.65 (d, 4H, J = 8.3 Hz), 8.31 (d, 2H, J = 8.8 Hz), 8.28 (s, 4H), 8.13 (d, 2H, J = 5.0 Hz), 8.08 (d, 2H J = 2.9 Hz), 8.00 (d, 2H, J = 4.8 Hz),

7.69-7.62 (m, 6H). HR-MS Calcd for $C_{41}H_{25}N_{10}ClRu$ (**2** - $2PF_6$): 394.05086 Da, found 394.05131 Da.

$[Ru(TAP)_2CPIP].2PF_6$ **3.** $[Ru(TAP)_2Cl_2]$ (20 mg, 0.037 mmol) and CPIP (15 mg, 0.045 mmol) were dissolved in ethylene glycol (3 mL) and heated at 120°C for 20h in the dark and under argon. After cooling and addition of aqueous solution of NH_4PF_6, a solid was formed. The latter was washed 3 times with water, EtOH and Et_2O to afford the final pure product as an orange powder (34 mg, 83%). ^{1}H-NMR (500 MHz, CD_3CN): δ (ppm) 9.01-8.94 (m, 6H), 8.62 (s, 4H), 8.27 (d, 2H, J = 8.6 Hz), 8.24 (d, 2H, J = 2.8 Hz), 8.19 (d, 2H, J = 2.7 Hz), 8.04 (d, 2H, J = 4.3 Hz), 7.73 (dd, 2H, J = 8.3 Hz, J = 5.3 Hz), 7.66 (d, 2H, J = 8.6 Hz). HR-MS Calcd for $C_{39}H_{23}N_{12}ClF_6PRu$ (**3** - $1PF_6$): 941.053699 Da, found 941.054467 Da.

$[Ru(TAP)_2CPITAP].2PF_6$ **4.** $[Ru(TAP)_2Cl_2]$ (20 mg, 0.037 mmol) and CPITAP (15 mg, 0.044 mmol) were dissolved in ethylene glycol (3 mL) and heated at 120°C for 20h in the dark and under argon. After cooling and addition of aqueous solution of NH_4PF_6, a solid was formed. The latter was washed 3 times with water, EtOH and Et_2O to afford the crude product. Purification over preparative SiO_2 chromatography ($CH_3CN/H_2O/KNO_{3(sat)}$ 7/2/1, v/v/v) gave the final product as a red powder (10 mg, 25%). ^{1}H-NMR (500MHz, CD_3CN): δ (ppm) 9.01-8.98 (m, 4H), 8.97 (d, 2H, J = 2.8 Hz), 8.64 (s, 4H), 8.32 (d, 2H, J = 8.6 Hz), 8.29 (s, 2H), 8.24 (d, 2H, J = 2.7 Hz), 8.15 (d, 2H, J = 2.8 Hz), 7.66 (d, 2H, J = 8.5 Hz). HR-MS Calcd for $C_{37}H_{21}N_{14}ClRu$ (**4** - $2PF_6$): 396.04136 Da, found 396.04171 Da.

Absorption and luminescence studies.

UV-vis absorption spectra were recorded on a Shimadzu UV-1700. The concentration of the complexes was 50 μM. Room temperature luminescence spectra were recorded on a Varian Cary Eclipse instrument. Luminescence intensity at 77 K was recorded on a FluoroLog3 FL3-22 from Jobin Yvon equipped with an 18 V 450 W Xenon Short Arc lamp and an R928P photomultiplier, using an Oxford Instrument Optistat DN nitrogen cryostat controlled by an Oxford Intelligent Temperature Controller

(ITC503S) instrument. Quantum yield were obtained using $[Ru(bpy)_3]^{2+}$ as a reference.[51] Luminescence lifetime measurements were performed after irradiation at λ = 400 nm obtained by the second harmonic of a Titanium:Sapphire laser (picosecond Tsunami laser spectra physics 3950-M1BB+39868-03 pulse picker doubler) at a 80 kHz repetition rate. The Fluotime 200 from AMS technologies was used for the decay acquisition. It consists of a GaAs microchannel plate photomultiplier tube (Hamamatsu model R3809U-50) followed by a time-correlated single photon counting system from Picoquant (PicoHarp300). The ultimate time resolution of the system is close to 30 ps. Luminescence decays were analysed with FLUOFIT software available from Picoquant.

Electrochemical studies.

Cyclic voltammetry was carried out in a one-compartment cell, using a glassy carbon disk working electrode (approximate area = 0.03 cm^2), a platinum wire counter electrode, and an Ag/AgCl reference electrode. The potential of the working electrode is controlled by an Autolab PGSTAT 100 potentiostat through a PC interface. The cyclic voltammograms were recorded with a sweep rate of 100 mV s^{-1}, in dried acetonitrile (Sigma-Aldrich, HPLC grade). The concentration of the complexes was 8.10^{-4} mol/L, with 0.1 mol/L tetrabutylammonium perchlorate as supporting electrolyte. Before each measurement, the samples were purged by nitrogen. Redox potentials were controlled by comparison with ferrocene, added at the end of the measurement.

Luminescence titration.

dGMP titration experiment of complexes **1-3** were recorded on a Varian Cary Eclipse instrument. A solution of dGMP (5 mM) was progressively added to a solution of complex (50 µM) in 50 mM Tris-HCl buffer, pH = 7.4. Luminescence titration with ODN (GC rich hairpin or wtTel23 G-quadruplex DNA) spectra were recorded in 10 mM HEPES, 35 mM NaCl, 50 mM KCl (pH=7.4) buffer on a Varian Cary Eclipse instrument for complex **1** and **3**; and on a FluoroLog3 FL3-22 from Jobin Yvon for

complex **2**. The titration was performed from the highest DNA concentration (10 µM) and progressively decreased it whereas the complex concentration (5 µM) was kept constant. The fitting equations are described in the Supporting Information.

CD experiments.

Prior to CD analysis, the oligonucleotides were annealed by heating the sample at 95°C for 5 min in the buffer conditions and cooling it overnight to room temperature. Analyses were recorded on a Jasco J-810 spectro-polarimeter using 1 cm length quartz cuvette. Spectra were recorded in a range of 5 from 25°C to 90°C with a wavelength range of 220 to 330 nm. For each temperature, the spectrum was an average of three scans with a 0.5 s response time, a 1 nm data pitch, a 4 nm bandwidth and a 200 nm min^{-1} scanning speed. For CD melting experiments, the ellipticity was recorded at 290 and 252 nm for wtTel23 and duplex hairpin, respectively. Melting temperatures were obtained using Boltzmann fit on Origin software. Each curve fit was only accepted with a r_{value}>0.99.

Bio layer interferometry (BLI).

BLI sensors coated with streptavidin (SA sensors) were purchased from Forte Bio (PALL). Prior to use, they were immerged 10 minutes in buffer before functionalization to dissolve the sucrose layer. Then the sensors were dipped for 15 minutes in DNA containing solutions (biotinylated systems **A**-**D**) at 100 nM and rinsed in buffer solution (10 mM HEPES pH 7.4, 35 mM NaCl, 50 mM KCl and 0.5% v/v surfactant P_{20}) for 10 minutes. The functionalized sensors were next dipped in different ruthenium complex containing solution at different concentrations (see the Supporting Information) for 2 minutes interspersed by a rinsing step in the buffer solution during 4 minutes. Reference sensors without DNA immobilization were used to subtract the non-specific adsorption on the SA layer. The sensorgrams were fitted using a heterogeneous model (see sensorgrams in Figures S39-S42). The reported values are the means of representative independent experiments, and the errors provided are standard deviations

from the mean. Each experiment was repeated at least two times.

Computational studies.

The docking experiments were performed with complex **3** which geometry was first optimized at the B3LYP/6-31g* level using the Gaussian09 software. Then, the AutoDock 4.0 software package was used on the crystal structure of parallel quadruplexes from human telomeric DNA (PDB entry: 1KF1). A grid of 80x80x80 points with a spacing of 0.5 Å between the grid points was used, non-polar hydrogens were merged and Gasteiger-Hückel charges were added on both the complex and the G-quadruplex. The parameters for the Ru atom were set on r=2.96 Å, q=+2.0 and the van der Waals well depth was 0.056 kcal.mol^{-1}. The docking calculations were obtained through a genetic algorithm search generating one hundred docked structures. A default protocol was applied with an initial population of 150 randomly placed individuals, a maximum number of 2.5x10^5 energy evaluations, a maximum number of 2.7x10^4 generations, a mutation rate of 0.02, and a crossover rate of 0.8. Results differing by less than 2 Å in positional root-mean-square-deviation (RMSD) were clustered together and represented the result with the most favourable free binding energy. Regarding the molecular mechanics dynamic simulation, the AMBER 12 software package was chosen and applied on the two best-ranked positions obtained from the docking calculations. The complex was broken down into its different ligands and their specific parameters were generated via the ANTECHAMBER module and the GAFF force field whereas charges were calculated through a RESP fitting of HF/6-31g* level calculations. The docking structures were solvated in a TIP3P water box which dimension was set to be at least 10 Å larger than the solute in every direction. Sodium cations were added until global charge was neutral and long-range electrostatic interactions were computated using the particle-mesh Ewald method with a cut-off value of 10 Å. After minimization and heating, an MD simulation was run at 300 K for 20 ns with time step set at 1 fs.

Confocal laser scanning microscopy.

U2OS cells were grown at 37 °C in a humidified atmosphere with 5 % CO_2 in DMEM medium (Westburg) containing 10% foetal bovine serum (FBS) (Gibco) and 1% penicillin/streptomycin (Westburg). 20 000 cells were seeded onto coated microscope slide and incubated with 20 µM of complex **1** for 24 h in the dark. After incubation, the medium containing the complex was removed, and fresh medium was added to the cells. The cells were rinsed in pre-warmed PBS, fixed in 4 % paraformaldehyde (VWR) for 10 min, labelled with Draq5 (eBioscience) following the instructions of the manufacturer. A confocal laser scanning microscopy system (Zeiss LSM 710) was used to acquire the images. Pictures were processed with Zen software.

Photocytotoxicity experiments.

U2OS cells were cultured in 96-well plates for 24h in DMEM (Westburg) containing 10% fetal bovine serum (FBS) (Gibco) and 1% penicillin/streptomycin (Westburg) to reach a density of 10 000 cells/well. The medium was removed and fresh one containing 10 µM of the complexes was added. After 24 h of incubation at 37 °C in the dark, cells were rinsed twice with PBS to remove non-internalized complexes. Illumination was performed during 30 minutes with blue LED (LED strip IP68 60 LED/m from Prolumia, 405 nm at 15.7 W/m^2). The distance between the light source and the culture plate was of 10 cm. Before illumination, cultures were rinsed with PBS and illuminated in PBS to avoid absorption by coloured culture medium. Plates serving as a dark control were protected from illumination with alumina foil. Illuminated and control cultures were put back immediately to the incubator at 37 °C in a humidified environment and cultured in fresh culture medium for an additional 24 h. The cell viability was measured 1 day post-irradiation using 10 µl/well of WST-1 reagent (Sigma-Aldrich) following the manufacturer's instructions. The ratio of the optical density at λ = 450 nm under each set of conditions relative to that of control cells (non-transfected and non-irradiated, 100% viability) was used to

determine a relative viability. The measurements were performed twelve times.

ASSOCIATE CONTENT

Copies of NMR and MS spectra, absorption and luminescence spectra, cyclic voltammograms, CD, BLI and SPR sensorgrams and cells microscopy.

AUTHOR INFORMATION

Corresponding Authors

* Benjamin.Elias@uclouvain.be

* Eric.Defrancq@univ-grenoble-alpes.fr

ORCID

Benjamin Elias: /0000-0001-5037-3313

Eric Defrancq: /0000-0002-3911-6241

Notes

The authors declare no competing financial interest.

Acknowledgements

J.W., M.A., L.M. and B.E. gratefully acknowledge the "*Fonds National pour la Recherche Scientifique"* (F.R.S.-FNRS), the "*Fonds pour la Formation à la Recherche dans l'Industrie et dans l'Agriculture"* (F.R.I.A.), the "*Région Wallonne"*, the "*Université catholique de Louvain"* and the "*Prix Pierre et Colette Bauchau"* for financial support. This work was supported by the "*Agence National de la Recherche*" (ANR-12-BSV8-0008-04 and ANR-16-CE11-0006-01), Labex ARCANE (ANR-11-LABX-0003-01) and the Région Auvergne-Rhône-Alpes. The NanoBio-ICMG platforms (FR 2607) are

acknowledged for their support. We also thank Dr L. Troian-Gautier for the scientific advice in the synthesis of CPITAP, Dr L. Bonnat and Dr T. Lavergne for providing biomolecular systems **A-D**, and Professor F. Loiseau for the help in the measurements of the luminescence lifetimes. M.-C. Eloy is thanked for the help about confocal microscopy experiments.

References

1. D. R. Boer, A. Canals, M. Coll, *Dalton Trans.* **2009**, *3*, 399-414.
2. H. J. Lipps, D. Rhodes, *Trends Cell Biol.* **2009**, *19*, 414-422.
3. M. L. Bochman, K. Paeschke, V. A. Zakian, *Nat. Rev. Genet.* **2012**, *13*, 770-780.
4. T. Simonsson, *Biol. Chem.* **2001**, *382*, 621-628.
5. A. Siddiqui-Jain, C. L. Grand, D. J. Bearss, L. H. Hurley, *Proc. Natl. Acad. Sci. USA* **2002**, *99*, 11593-11598.
6. M. Métifiot, S. Amrane, S. Litvak, M.-L. Andreola, *Nucleic Acids Res.* **2014**, *42*, 12352-12366.
7. G. Biffi, M. Di Antonio, D. Tannahill, S. Balasubramanian, *Nat. Chem.* **2013**, *6*, 75-80.
8. G. Biffi, D. Tannahill, J. McCafferty, S. Balasubramanian, *Nat. Chem.* **2013**, *5*, 182-186.
9. A. Laguerre, K. Hukezalie, P. Winckler, F. Katranji, G. Chanteloup, M. Pirrotta, J.-M. Perrier-Cornet, J. M. Y. Wong, D. Monchaud, *J. Am. Chem. Soc.* **2015**, *137*, 8521-8525.
10. A. De Cian, L. Lacroix, C. Douarre, N. Temime-Smaali, C. Trentesaux, J.-F. Riou, J.-L. Mergny, *Biochimie* **2008**, *90*, 131-155.
11. D. J. Patel, A. T. Phan, V. Kuryavyi, *Nucleic Acids Res.* **2007**, *35*, 7429-7455.
12. D. Hanahan, R. A. Weinberg, *Cell* **2011**, *144*, 646-674.
13. T. M. Bryan, A. Englezou, L. Dalla-Pozza, M. A. Dunham, R. R. Reddel, *Nat. Med.* **1997**, *3*, 1271-1274.

14. A. J. Cesare, R. R. Reddel, *Nat. Rev. Genet.* **2010**, *11*, 319-330.
15. H. Han, L. H. Hurley, *Trends Pharmacol. Sci.* **2000**, *21*, 136-142.
16. D. Monchaud, M.-P. Teulade-Fichou, *Org. Biomol. Chem.* **2008**, *6*, 627-636.
17. P. Murat, Y. Singh, E. Defrancq, *Chem. Soc. Rev.* **2011**, *40*, 5293-5307.
18. D. Yang, K. Okamoto, *Future Med. Chem.* **2010**, *2*, 619-646.
19. B. R. Vummidi, J. Alzeer, N. W. Luedtke, *ChemBioChem* **2013**, *14*, 540-558.
20. S. Neidle, *Nat. Rev. Chem.* **2017**, *1*, 0041.
21. M. Nadai, F. Doria, L. Germani, S. N. Richter, M. Freccero, *Chem. Eur. J.* **2015**, *21*, 2330-2334.
22. S. N. Georgiades, N. H. Abdkarim, K. Suntharalingam, R. Vilar, *Angew. Chem. Int. Ed.* **2010**, *49*, 4020-4034.
23. Q. Cao, Y. Li, E. Freisinger, P. Z. Qin, R. K. O. Sigel, Z.-W. Mao, *Inorg. Chem. Front.* **2017**, *4*, 10-32.
24. R. Kieltyka, P. Englebienne, J. Fakhoury, C. Autexier, N. Moitessier, H. F. Sleiman, *J. Am. Chem. Soc.* **2008**, *130*, 10040-10041.
25. K. J. Castor, Z. Liu, J. Fakhoury, M. A. Hancock, A. Mittermaier, N. Moitessier, H. F. Sleiman, *Chem. Eur. J.* **2013**, *19*, 17836-17845.
26. D. L. Ang, B. W. J. Harper, L. Cubo, O. Mendoza, R. Vilar, J. Aldrich-Wright, *Chem. Eur. J.* **2016**, *22*, 2317-2325.
27. S. Ghosh, O. Mendoza, L. Cubo, F. Rosu, V. Gabelica, A. J. P. White, R. Vilar, *Chem. Eur. J.* **2014**, *20*, 4772-4779.
28. M. Trajkovski, E. Morel, F. Hamon, S. Bombard, M.-P. Teulade-Fichou, J. Plavec, *Chem. Eur. J.* **2015**, *21*, 7798-7807.
29. N. H. Campbell, N. H. A. Karim, G. N. Parkinson, M. Gunaratnam, V. Petrucci, A. K. Todd, R.

Vilar, S. Neidle, *J. Med. Chem.* **2012**, *55*, 209-222.

30. C. Q. Zhou, T. C. Liao, Z. Q. Li, J. Gonzalez-Garcia, M. Reynolds, M. Zou, R. Vilar, *Chem. Eur. J.* **2017**, *23*, 4713-4722.
31. A. Ali, M. Kamra, S. Roy, K. Muniyappa, S. Bhattacharya, *Bioconj. Chem.* **2017**, *28*, 341-352.
32. X. Chen, J. H. Wu, Y. W. Lai, R. Zhao, H. Chao, L. N. Ji, *Dalton Trans.* **2013**, *42*, 4386-4397.
33. L. Xu, X. Chen, J. Wu, J. Wang, L. Ji, H. Chao, *Chem. Eur. J.* **2015**, *21*, 4008-4020.
34. X. Wang, L. Pei, X. Fan, S. Shi, *Inorg. Chem. Comm.* **2016**, *72*, 7-12.
35. S. Lin, L. Lu, T.-S. Kang, J.-L. Mergny, C.-H. Leung, D.-L. Ma, *Anal. Chem.* **2016**, *88*, 10290-10295.
36. K. J. Castor, K. L. Metera, U. M. Tefashe, C. J. Serpell, J. Mauzeroll, H. F. Sleiman, *Inorg. Chem.* **2015**, *54*, 6958-6967.
37. L. Lu, M. Wang, Z. Mao, T.-S. Kang, X.-P. Chen, J.-J. Lu, C.-H. Leung, D.-L. Ma, *Scientific Rep.* **2016**, *6*, 22458.
38. F. E. Poynton, S. A. Bright, S. Blasco, D. C. Williams, J. M. Kelly, T. Gunnlaugsson, *Chem. Soc. Rev.*, **2017**, *46*, 7706-7756.
39. Q. Deraedt, L. Marcelis, F. Loiseau, B. Elias, *Inorg. Chem. Front.* **2017**, *4*, 91-103.
40. A. N. Boynton, L. Marcélis, A. J. McConnell, J. K. Barton, *Inorg. Chem.* **2017**, *56*, 8381-8389.
41. G. Piraux, L. Bar, M. Abraham, T. Lavergne, H. Jamet, J. Dejeu, L. Marcélis, E. Defrancq, B. Elias, *Chem. Eur. J.*, **2017**, *23*, 11872-11880.
42. A. Masschelein, L. Jacquet, A. Kirsch-De Mesmaeker, J. Nasielski, *Inorg. Chem.* **1990**, *29*, 855-860.
43. L. Marcélis, J. Ghesquière, K. Garnir, A. Kirsch-De Mesmaeker, C. Moucheron, *Coord. Chem. Rev.* **2012**, *256*, 1569-1582.

44. C. S. Burke, A. Byrne, T. E. Keyes, *J. Am. Chem. Soc.* **2018**, *140*, 6945-6955.

45. S. M. Cloonan, R. B. P. Elmes, M. Erby, S. A. Bright, F. E. Poynton, D. E. Nolan, S. J. Quinn, T. Gunnlaugsson, D. C Williams, *J. Med. Chem.* **2015**, *58*, 4494-4505.

46. S. Rickling, L. Ghisdavu, F. Pierard, P. Gerbaux, M. Surin, P. Murat, E. Defrancq, C. Moucheron, A. Kirsch-De Mesmaeker, *Chem. Eur. J.* **2010**, *16*, 3951-3961.

47. F. Heinemann, J. Karges, G. Gasser, *Acc. Chem. Res.* **2017**, *50*, 2727-2736.

48. K. J. Castor, J. Mancini, J. Fakhoury, N. Weill, R. Kieltyka, P. Englebienne, N. Avakyan, A. Mittermaier, C. Autexier, N. Moitessier, H. F. Sleiman, *ChemMedChem* **2012**, *7*, 85-94.

49. L. Herman, S. Ghosh, E. Defrancq, A. Kirsch-De Mesmaeker, *J. Phys. Org. Chem.* **2008**, *21*, 670-681.

50. I. Ortmans, B. Elias, J. M. Kelly, C. Moucheron, A. Kirsch-De Mesmaeker, *Dalton Trans.* **2004**, *4*, 668-676.

51. A. M. Brouwer, *Pure Appl. Chem*. **2011**, *83*, 2213-2228.

52. B. Elias, A. Kirsch-De Mesmaeker, *Coord. Chem. Rev.* **2006**, *250*, 1627-1641.

53. S. P. Foxon, M. A. H. Alamiry, M. G. Walker, A. J. H. M. Meijer, I. V. Sazanovich, J. A. Weinstein, J. A. Thomas, *J. Phys. Chem. A*, **2009**, *113*, 12754-12762.

54. A. Boisdenghien, C. Moucheron, A. Kirsch-De Mesmaeker, *Inorg. Chem.* **2005**, *44*, 7678-7685.

55. S. Steenken, S. V. Jovanovic, *J. Am. Chem. Soc.* **1997**, *119*, 617-618.

56. J. Wallner, G. Lhota, D. Jeschek, A. Mader, K. Vorauer-Uhl, *J. Pharm. Biomed. Anal.* **2013**, *72*, 150-154.

57. P. Murat, R. Bonnet, A. Van-der-Heyden, N. Spinelli, P. Labbé, D. Monchaud, M.-P. Teulade-Fichou, P. Dumy, E. Defrancq, *Chem. Eur. J.* **2010**, *16*, 6106-6114.

58. R. Bonnet, T. Lavergne, B. Gennaro, N. Spinelli, E. Defrancq, *Chem. Comm.* **2015**, *51*, 4850-4853.

59. P. Murat, D. Cressend, N. Spinelli, A. Van der Heyden, P. Labbé, P. Dumy, E. Defrancq, *ChemBioChem* **2008**, *9*, 2588-2591.
60. L. Bonnat, L. Bar, B. Génnaro, H. Bonnet, O. Jarjayes, F. Thomas, J. Dejeu, E. Defrancq, T. Lavergne, *Chem. Eur. J.* **2017**, *23*, 5602-5613.
61. L. Bonnat, J. Dejeu, H. Bonnet, B. Génnaro, O. Jarjayes, F. Thomas, T. Lavergne, E. Defrancq, *Chem. Eur. J.* **2016**, *22*, 3139-3147.
62. C. M. Incles, C. M. Schultes, H. Kempski, H. Koehler, L. R. Kelland, S. Neidle, *Mol. Cancer Therapeutic* **2004**, *3*, 1201-1206.
63. The other complexes could not be used because of their lower quantum yield of emission (complex **2**) or their photo-reactivity (complexes **3** and **4** undergo PET with guanine residues which quenches the excited state). Their luminescence in the cells is thus too weak to be detected by confocal microscopy.
64. L. Jacquet, A. Kirsch-De Mesmaeker, *J. Chem. Soc, Faraday Trans.* **1992**, *88*, 2471-2480.
65. C. Hiort, P. Lincoln, B. Norden, *J. Am. Chem. Soc.* **1993**, *115*, 3448-3454.
66. C. Moucheron, A. Kirsch-De Mesmaeker, S. Choua, *Inorg. Chem.* **1997**, *36*, 584-592.